# Thin, Millimeter Scale Fingernail Sensors for Thermal Characterization of Nail Bed Tissue

*Yajing Li, Yinji Ma, Chen Wei, Haiwen Luan, Shuai Xu, Mengdi Han, Hangbo Zhao, Cunman Liang, Quansan Yang, Yiyuan Yang, Kaitlyn E. Crawford, Xue Feng, Yonggang Huang,\* and John A. Rogers\**

Thin, flexible, body-worn technologies that allow precise, quantitative monitoring of physiological status are of broad current interest due to their potential to improve the cost and effectiveness of healthcare. Although the surface of the skin represents one of the most widely explored points of integration, recently developed millimeter scale wireless sensor platforms allow deployment on alternative surfaces of the body, such as the finger/toenails and the teeth. The work described here introduces a collection of ideas in materials science, device engineering and computational techniques that enables precise characterization of the thermal transport characteristics of the nail bed tissue from measurements on the surface of the nail. Systematic in vitro studies demonstrate the underlying measurement principles, the theoretical models for optimized sensor design and the associated experimental procedures for determining the thermal conductivity of the tissue. Measurements performed on human subjects highlight capabilities in tracking changes in perfusion of the nail bed tissues in response to various external stimuli.

## 1. Introduction

In clinical medicine, the nail unit is a well-known, useful source of information on health status and an important component of the physical exam.[1–3] Any alterations in the nature of the nail plate, the nail matrix, the hyponychium, the proximal nail fold, the lateral nail folds or the nail bed, may reflect nutritional, endocrine, congenital, infectious, neoplastic, traumatic, inflammatory or vascular imbalances both locally and systemically. The optical transparency of the nail plate allows this structure to serve as a noninvasive window into microvascular integrity through direct visualization of nail fold capillaries. As such, noninvasive and point-of-care tools such as digital

Dr. Y. Li
Department of Materials Science and Engineering
Center for Bio-Integrated Electronics
Northwestern University
Evanston, IL 60208, USA

Dr. Y. Ma, Prof. X. Feng
Department of Engineering Mechanics
Center for Mechanics and Materials
Tsinghua University
Beijing 100084, China

C. Wei, H. Luan
Department of Civil and Environmental Engineering,
Mechanical Engineering, Materials Science and Engineering
Northwestern University
Evanston, IL 60208, USA

Dr. S. Xu
Center for Bio-Integrated Electronics
Department of Dermatology
Feinberg School of Medicine
Northwestern University
Evanston, IL 60208, USA

Dr. M. Han, Dr. H. Zhao, C. Liang, Q. Yang, Y. Yang
Center for Bio-Integrated Electronics
Northwestern University
Evanston, IL 60208, USA

The ORCID identification number(s) for the author(s) of this article can be found under https://doi.org/10.1002/adfm.201801380.

Prof. K. E. Crawford
Department of Materials Science and Engineering
Burnett School of Biomedical Sciences
University of Central Florida
Orlando, FL 32827, USA

Prof. Y. Huang
Department of Civil and Environmental Engineering,
Mechanical Engineering, Materials Science and Engineering
Skin Disease Research Center
Feinberg School of Medicine
Northwestern University
Evanston, IL 60208, USA
E-mail: y-huang@northwestern.edu

Prof. J. A. Rogers
Departments of Materials Science and Engineering,
Biomedical Engineering, Chemistry, Mechanical Engineering,
Electrical Engineering and Computer Science, and
Neurological Surgery
Center for Bio-Integrated Electronics
Simpson Querrey Institute for Nano/biotechnology
Northwestern University
Evanston, IL 60208, USA
E-mail: jrogers@northwestern.edu

platforms for dermoscopy and proximal nail fold capillaroscopy serve as diagnostic instruments in the evaluation of connective tissue diseases (e.g., Raynaud's phenomenon and systemic sclerosis[4]) and nail tumors.[5] Operation of these technologies and interpretation of data collected with them require, however, clinical expertise and they cannot be used for continuous monitoring outside of a hospital or laboratory setting.

Recent work shows that advanced imaging techniques such as ultrasound, CT (computed tomography), MRI (magnetic resonance imaging), and PET (positron emission tomography) can be used to examine the dynamics and structure of tissues of the fingers and nails for diagnostic purposes. Although modern imaging technologies allow for visualization of multiparameter data at multidimensional resolution, these systems are expensive and have limited utility at the point-of-care. While cutaneous skin biopsies are largely noninvasive and straightforward, tissue sampling of the nail unit is a complex procedure that often requires nail avulsion, postoperative discomfort, along with risk of infection, and long-term nail dystrophy.[6,7] Thus, technologies that can derive additional information from the nail unit noninvasively at the point-of-care and/or in a continuous monitoring mode without significant cost or complex imaging systems could offer significant clinical value for both diagnosis and treatment management. Beyond acting as a useful source of clinical information, the nail unit also represents an ideal, hard, and mechanical interface for mounting and bonding advanced device technologies. Specifically, the nail plate is a semitransparent material composed of cornified keratinocytes and keratin proteins, which imparts significant mechanical strength and resistance to environmental insult.[8] This construction enables stable coupling of sensors and devices with the human body without the risk of irritation, redness, or allergic reactions. Furthermore, the nail plate grows slowly at ≈1 to 3 mm per month, thereby allowing long-term sensing.[9]

Advanced sensing techniques developed for skin-like, or "epidermal," electronics use precision thermal sensors and actuators to determine thermal transport properties of living tissues in a real-time, noninvasive fashion.[10–13] These systems integrate metallic filaments with soft, thin supporting substrates to allow operation while in intimate contact with curvilinear skin, without irritation or sensory perception at the skin interface. Direct measurement of the body surface temperature and quantification of the thermal transport properties (i.e., thermal conductivity) associated with physiological conditions such as perfusion and hydration level are both possible, with clinical-grade accuracy. Past demonstrations focused on characterization of the upper layer of the skin,[10–13] without consideration of its naturally layered structure or its properties significantly below the surface. The assessment of the thermal characteristics of deep tissues is challenging and of great interest. Here,

we present a noninvasive method of exploiting nail-mounted thermal sensors to measure the thermal conductivity of the nail bed, independent of the thermal properties of the nail. Combined with thermal analysis techniques, the responses of such sensors provide quantitative information of the perfusion of the nailbed tissue, and of other processes that alter the thermal transport characteristics. These thin, miniaturized devices yield data of direct relevance to physiological health and offer the potential for continuous monitoring as an unusual class of wearable technology with integration of wireless power source and data communication functionality.

## 2. Results and Discussions

**Figure 1**a presents an exploded view illustration of a representative fingernail sensor for temperature and thermal transport. The devices involve a multilayer construction, where the two active areas (one with radius 0.5 mm and the other 1.5 mm; each serves simultaneously as a temperature sensor and a thermal actuator) consist of lithographically defined, narrow (10 µm) traces of gold in spiral disk geometries, as highlighted in Figure 1b. The traces for each disk emerge at the edges into wide (≈0.8 mm) ribbons that lead to contact pads as interfaces to external electronics for control and data acquisition. Layers of polyimide (3 µm thickness) encapsulate these conductive traces from above and below as barriers to biofluids and water, thereby also positioning them at the neutral mechanical plane for enhanced bendability. A thin (200 µm) sheet of a silicone
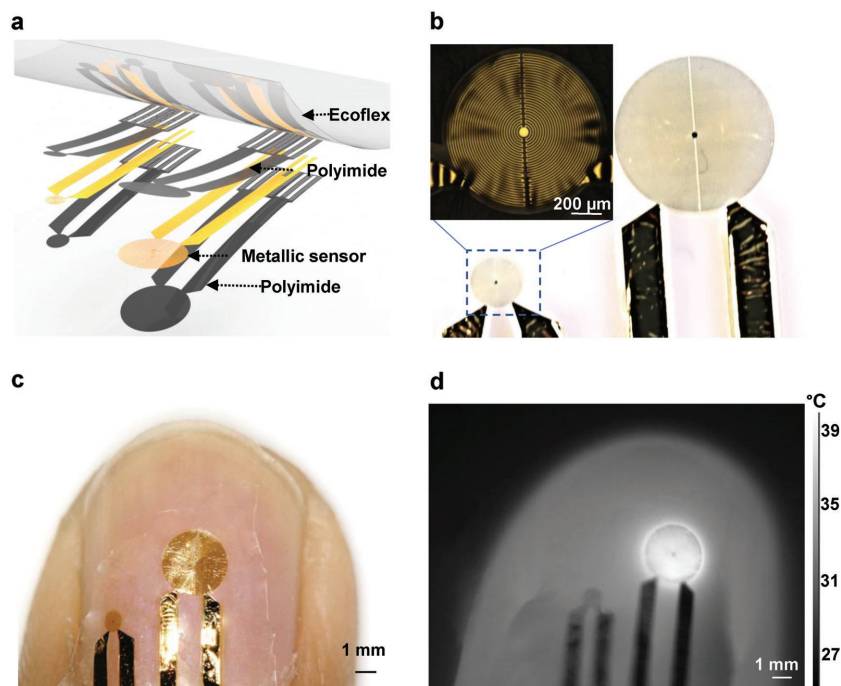


**Figure 1.** Thin, flexible thermal sensors that laminate onto the surfaces of the fingernails enable measurements of the thermal transport properties of the nail bed tissues. a) Exploded view schematic illustration of a representative device that includes a small (radius ≈0.5 mm) and a large (radius ≈1.5 mm) sensor. b) Optical image of a device. The inset provides a magnified view of the small sensor. c) Optical image of the sensor platform laminated on a fingernail and d) the corresponding infrared image during operation.

elastomer serves as a mechanical support for handling and manipulation. The low modulus of this material and its tacky surface ensure intimate, conformal contact, and therefore efficient thermal coupling, to the nail via reversible van der Waals interactions.

The devices connect to a power supply (6220, Keithley Instrument) and a digital multimeter (DMM, National Instruments) to allow delivery of controlled, direct current (DC) inputs to the sensors/actuators and simultaneous measurements of their resistance. In this way, the devices serve simultaneously as thermal actuators and temperature sensors. The resulting measurement physics relies on the well-established transient plane source (TPS) method.[14] Briefly, the active element in the TPS approach delivers thermal power to the sample via Joule heating that results from application of DC current. The same device simultaneously enables time-dependent measurements of resulting changes in temperature through the temperature coefficient of resistance (TCR) of the metal. Data recorded in this manner can be combined with computational techniques to determine the intrinsic thermal transport properties, i.e., the thermal conductivity and thermal diffusivity, of the material under test. Figure 1d shows an infrared image of the devices operating in this manner on the surface of the fingernail.

The fingernail consists of a rigid plate (typically with thickness ≈0.5 mm that varies by only ≈50 µm from the proximal to distal end)[15–17] mechanically and thermally coupled to the underlying tissue. The nail plate is made of alpha-keratin, with

thermal conductivity between ≈0.2 and 0.4 W m$^{-1}$ K$^{-1}$.[18] The nail bed is made of two types of tissues: the epidermis and the deeper dermis which includes rich capillaries and glands, with thermal conductivity between 0.2 and 0.5 W m$^{-1}$ K$^{-1}$.[19–23] Experiments to establish the basic operating principles of the sensors and the methods to interpret data collected by them use test platforms that consist of a thin film of silicone on a thick base layer of a silicone, each with a formulation to yield thermal properties and thicknesses comparable to those of skin tissues and nail plate. The corresponding computational modeling assumes a semi-infinite substrate.

The characteristic probing depth associated with the TPS method increases with the thermal diffusivity ($\alpha$) and the time for thermal actuation ($t$).[14,24,25] For a bilayer sample, characterization of the thermal properties of the bottom layer requires actuation times sufficient for heat to diffuse through the top layer. At long times, the temperature approximately saturates to a value that depends mainly on the thermal conductivity and only weakly on the thermal diffusivity.[14] **Figure 2**a illustrates the spatial-temporal characteristics of heat transport obtained by finite element analysis (FEA) for an actuator with radius, $R = 1.5$ mm and power density, $q = 3$ mW mm$^{-2}$ on a bilayer sample with a 0.5 mm thick top layer (thermal conductivity, $k_1 = 0.21$ W m$^{-1}$ K$^{-1}$; thermal diffusivity, $\alpha_1 = 0.15$ mm s$^{-2}$) and semi-infinite bottom layer ($k_2 = 0.44$ W m$^{-1}$ K$^{-1}$ and $\alpha_2 = 0.15$ mm s$^{-2}$). At short times (0.5 and 2 s), heat transport occurs mainly in the top layer, with little increase in temperature in
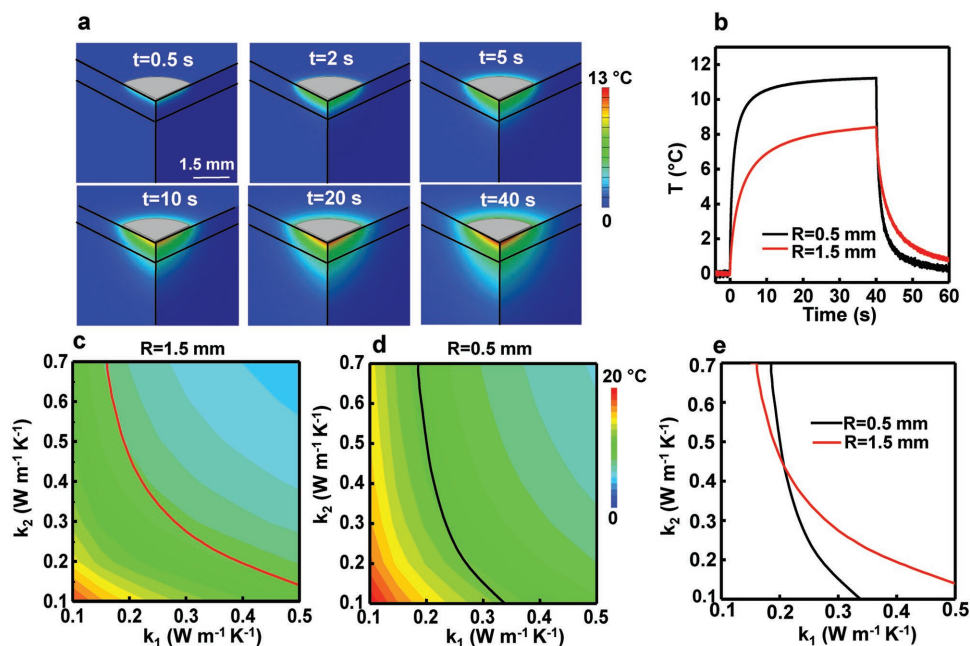


**Figure 2.** Summary of procedures to determine the thermal conductivities of a bilayer sample. a) FEA results (quarter, cross-sectional view) for the spatial distributions of increases in temperature induced by a thermal actuator placed on the surface of a bilayer sample at several times after actuation. The parameters in the FEA are $R = 1.5$ mm (radius of the actuator), $q = 3$ mW mm$^{-2}$ (thermal power from the actuator), $h = 0.5$ mm (thickness of the top layer), $k_1 = 0.21$ W m$^{-1}$ K$^{-1}$ (thermal conductivity of the top layer) and $k_2 = 0.44$ W m$^{-1}$ K$^{-1}$ (thermal conductivity of the base layer). b) Measured increases in temperature as a function of time for operation of actuators with $R = 0.5$ mm ($q = 10$ mW mm$^{-2}$) and 1.5 mm ($q = 3$ mW mm$^{-2}$). c,d) FEA results for the increases in temperature of the actuators at $t = 40$ s, $T_{ss}$, plotted as a function of $k_1$ and $k_2$, c) $R = 1.5$ mm and $q = 3$ mW mm$^{-2}$ and d) $R = 0.5$ mm and $q = 10$ mW mm$^{-2}$. The curves in panels (c) and (d) correspond to combinations of $k_1$ and $k_2$ that yield a certain value of $T_{ss}$. The color in these graphs corresponds to the values of $T_{ss}$ that result for other values $k_1$ and $k_2$. e) The point of intersection of the two curves in panels (c) and (d) yields $k_1$ and $k_2$.

**ADVANCED
SCIENCE NEWS**

www.advancedsciencenews.com

**ADVANCED
FUNCTIONAL
MATERIALS**

www.afm-journal.de

the bottom layer. At long times (20 and 40 s), the heat passes into both layers, and the temperature increase of the actuator saturates, as expected.

For a bilayer sample with a top layer whose thickness is known, the temperature increases associated with two actuators that have different radii, both operated in this long time (≈40 s) regime, can be used to determine $k_1$ and $k_2$. Figure 2b presents the measured temperature increase ($T$) of the actuator on a bilayer sample with a thin top layer (0.5 mm; Ecoflex) and thick bottom layer (13 mm; Sylgard 170) as a function of thermal actuation time for each of the two actuators operated with DC current (≈100 μA) for activation at 0 s and deactivation at 40 s. Measurements involve an enclosure around the sample to reduce fluctuations in temperature induced by convective heat transfer to the room. The quasi-steady state increase in temperature, i.e., $T$ at $t = 40$ s, or $T_{ss}$, is 11.0 °C for the small actuator ($R = 0.5$ mm and $q = 10$ mW mm$^{-2}$) and 8.4 °C for the large actuator ($R = 1.5$ mm and $q = 3$ mW mm$^{-2}$). Both values fall below the threshold for damaging tissue.[26,27] Figure 2c,d

shows the corresponding temperature increases of the two actuators (radii and powers specified in Figure 2b) obtained by FEA for different $k_1$ and $k_2$. FEA results yield curves that define pairs of $k_1$ and $k_2$ that are consistent with the experimentally measured $T_{ss}$ for both the small and the large actuator. The point of intersection of these two curves gives $k_1$ and $k_2$ for the bilayer sample, i.e., $k_1 = 0.21$ W m$^{-1}$ K$^{-1}$ for Ecoflex and $k_2 = 0.44$ W m$^{-1}$ K$^{-1}$ for Sylgard 170 in Figure 2e. These results are consistent with the literature values for these materials.[28,29] We selected sensors with radii of 0.5 and 1.5 mm since the small (large) sensor offers greater sensitivity to properties of the top (bottom) layers, as demonstrated in Figure S6 of the Supporting Information.

Measurements on samples with top layers that have different thicknesses further validate the measurement scheme. **Figure 3**a,b shows representative results ($R = 0.5$ mm and 1.5 mm, power $q = 10$ mW mm$^{-2}$ and 3 mW mm$^{-2}$, respectively) with top layer (Ecoflex) thicknesses between ≈300 and 600 μm (spatial variations of +/− 10 μm), each with the same
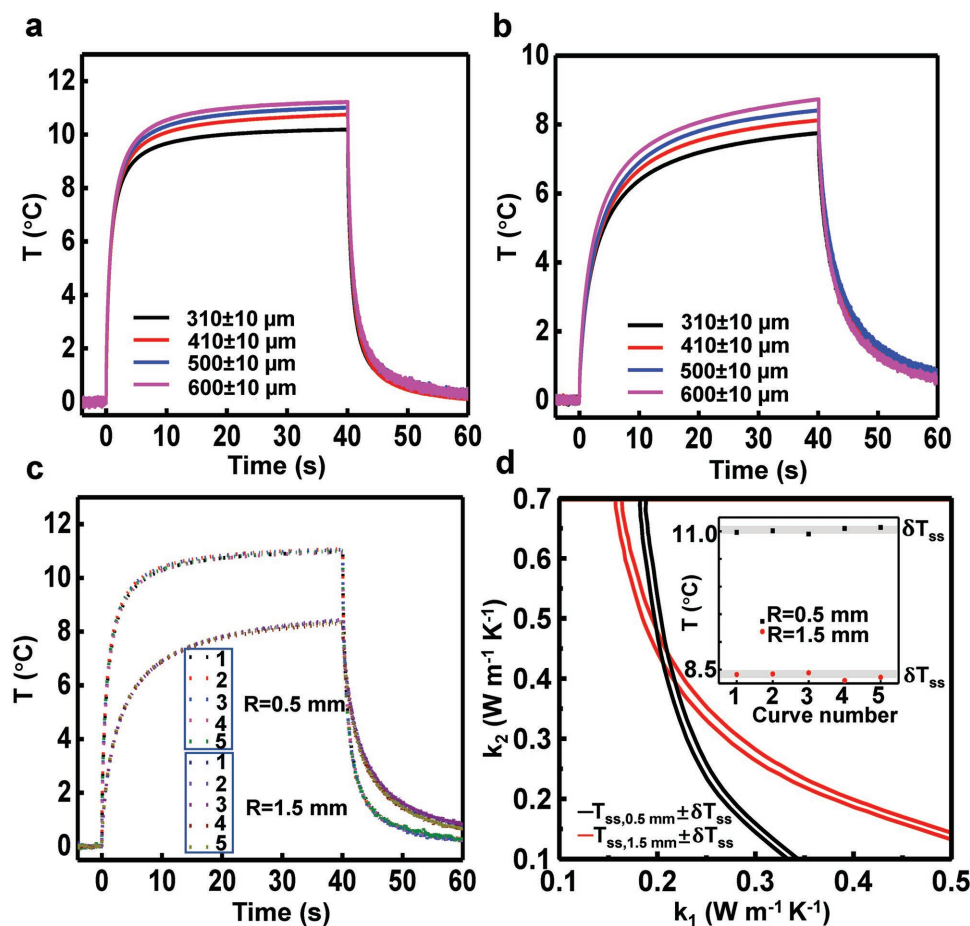


**Figure 3.** Experimental and computational results for the characterization of bilayer samples that consist of thin films (silicone, Ecoflex) with different thicknesses on a thick substrate (silicone, Sylgard 170), evaluated using sensors with radii, $R$, of 1.5 and 0.5 mm. a) Increase in temperature as a function of time for sensors with $R = 0.5$ mm and b) $R = 1.5$ mm, with bilayer samples that have different top layer thicknesses, with activation at 0 s and deactivation at 40 s. c) Increase in temperature measured with the two sensors as a function of time for repeated measurements on a sample with top layer thickness of 0.5 mm. d) Analysis of error and uncertainty in the parameters extracted from the data, determined by FEA. Each curve represents the measured value of $T_{ss}$ shifted by $\pm\delta T_{ss}$. The inset shows a magnified view of $T_{ss}$ of each curve in panel (c). The experimental variations in $T_{ss}$ lead to values of $\delta T_{ss}$ that are generally less than 0.1 °C. The points of intersection of these pairs of curves define the thermal conductivity values and their uncertainties, $k_{1,2} \pm \Delta k_{1,2}$.

type of bottom layer (Sylgard 170). Quasi-steady state temperatures, $T_{ss}$, analyzed using the scheme described previously yield values for the thermal conductivity. The results show consistent results, independent of the top layer thickness, i.e., $k_1 = 0.21$ W m$^{-1}$ K$^{-1}$, $k_2 = 0.42$ W m$^{-1}$ K$^{-1}$ for $h = 310$ μm; $k_1 = 0.21$ W m$^{-1}$ K$^{-1}$, $k_2 = 0.42$ W m$^{-1}$ K$^{-1}$ for $h = 410$ μm; $k_1 = 0.21$ W m$^{-1}$ K$^{-1}$, $k_2 = 0.44$ W m$^{-1}$ K$^{-1}$ for $h = 500$ μm; $k_1 = 0.21$ Wm$^{-1}$K$^{-1}$, $k_2 = 0.44$ W m$^{-1}$ K$^{-1}$ for $h = 600$ μm. Figure 3c and the inset in 3d show that the repeatability for $T_{ss}$ is ≈0.1 °C, roughly comparable to fluctuations in the ambient temperature (see Figure S2 of the Supporting Information). This value defines uncertainties in the extracted thermal conductivities, as summarized in Figure 3d. These uncertainties are consistent with the variations in values observed across samples with different top layer thicknesses, i.e., $k_1 = 0.21 \pm 0.01$ W m$^{-1}$ K$^{-1}$ and $k_2 = 0.44 \pm 0.04$ W m$^{-1}$ K$^{-1}$.
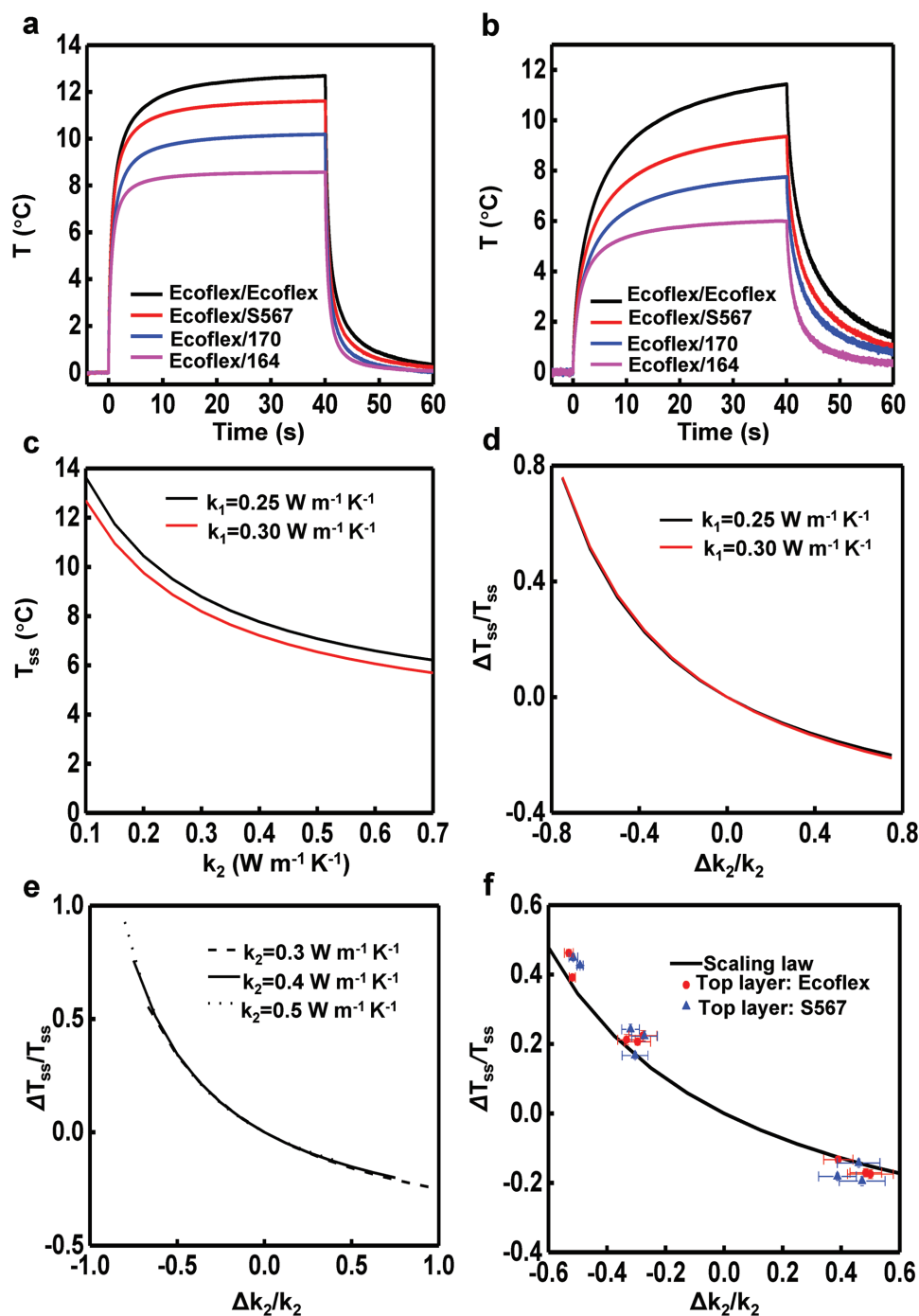
In many applications, the properties of the nail bed tissues are more important than those of the nail because they vary depending on physiological state. Measurements of changes in the thermal properties of the system are likely to be dominated by those of the tissue, as opposed to the nail. Studies of the sensitivity of the measurement to the bottom layer provide insights in this context. Here, the samples consist of bilayer structures with a fixed top layer (0.3 mm thick, Ecoflex) and various bottom layers (Ecoflex, Sylgard 567, Sylgard 170, and Sylgard 164), as summarized in **Figure 4**a,b. For both sensors, the Ecoflex/Ecoflex case yields values of $T_{ss}$ that are larger than those of Ecoflex/Sylgard567, Ecoflex/Slygard170, and Ecoflex/Sylgard164. The trends follow the thermal conductivities of the bottom materials ($k = 0.21 \pm 0.01$ W m$^{-1}$ K$^{-1}$ for Ecoflex, $k = 0.3 \pm 0.02$ W m$^{-1}$ K$^{-1}$ for Sylgard 567, $k = 0.44 \pm 0.04$ W m$^{-1}$ K$^{-1}$ for Sylgard 170, and $k = 0.66 \pm 0.01$ W m$^{-1}$ K$^{-1}$ for Sylgard 164).

Figure 4c presents a plot of $T_{ss}$ as a function of $k_2$ for $R = 1.5$ mm, $q = 3$ mW mm$^{-2}$, for two values of $k_1$. The curves clearly depend on $k_1$, which suggests that $k_2$ cannot be determined by using just one sensor/actuator if $k_1$ is unknown. Nevertheless, for physiological monitoring based on measurement of the nail and nail bed tissue, the change in $k_1$ can be assumed to be much smaller than the change in $k_2$. If $\Delta k_2$ and $\Delta T_{ss}$ are the change in $k_2$ and $T_{ss}$, respectively, then we can plot $\Delta T_{ss}/T_{ss}$ as a function of $\Delta k_2/k_2$ for several values of $k_1$ and $k_2$, as in Figure 4d,e. Remarkably, the results show that this relationship is only weakly dependent of $k_1$ (Figure 4d) and $k_2$ (Figure 4e) over this physiologically relevant range. As a result, $\Delta k_2/k_2$ can be determined directly from $\Delta T_{ss}/T_{ss}$, independent of the value of $k_1$ and $k_2$. This conclusion is clearly supported by experiments, as shown in Figure 4f, for different top-layer materials (Ecoflex and Sylgard567) and bottom-layer materials (Ecoflex, Sylgard567, Sylgard170, and Sylgard164). Here, the actuator radius and heating time are the same as those in the FEA in Figure 4c–e.

These studies establish a baseline of understanding that allows interpretation of data from these types of sensors used on human subjects (healthy female, age 29; left middle fingernail with nail thickness of $0.42 \pm 0.01$ mm measured with a caliper). **Figure 5**a shows measurement results from a single subject across 8 d of three repeated measurements performed in the afternoon on each day. To reduce the rates of convective heat transfer, measurements involve a piece of plastic foam to enclose the hand of the subject without touching the fingernail, as shown in Figure S5 of the supporting information. The thermal conductivity of the nail plate varies from 0.27 to 0.29 W m$^{-1}$ K$^{-1}$ over the observation period, in a narrow range consistent with values measured using other techniques.[18] The thermal conductivity of the nail bed varies more significantly, from 0.43 to 0.52 W mm$^{-2}$, as might be expected due to normal variations in hydration and surface blood flow, both of which can affect the thermal conductivity.[30,31] For instance, previous reports suggest that variations in blood flow can induce changes in thermal conductivity from 0.25 W m$^{-1}$ K$^{-1}$ (null blood flow) to 1 W m$^{-1}$ K$^{-1}$ (vasodilation).[32] These variations likely reflect the physiological changes, as opposed to variations that result from changes in the environment or the sensor response. Results in the Supporting Information show that repeated measurements on silicone samples over the course of 7 d reveal that variations in $T_{ss}$ are ≈0.1 °C, consistent with previously reported fluctuations in temperature.

Perfusion behaviors affect the distributions of temperature in living systems, with important purposes in thermoregulation. As such, perfusion is an important index for clinical procedures such as the treatment of tumors.[33] Abnormalities of peripheral microcirculation can play a central role in systemic sclerosis (SSc). Previous studies[10,11,21,34,35] indicate that the thermal conductivity of tissues can be strongly affected by micro and macrovascular blood flow. Figure 5b–f illustrates the temporal evolution of the thermal conductivity of the nail bed tissue as a result of changes in blood flow associated with a local, pressure induced occlusion of the blood vessels in the middle left finger of the subject (female, age 29). The measurements used a sensor with $R = 1.5$ mm laminated onto the center of the nail plate for continuous thermal characterization during and after the occlusion. Figure 5c presents the change in temperature of the nail plate of the left middle finger recorded by an infrared camera at the beginning of the period of occlusion. The results show that during the occlusion, the temperature decreases monotonically by >4 °C in the first 2 min followed by further reductions but with a reduced rate in the subsequent 7 min. The color of the finger turns gray and the pinkish tone of the tissue under the nail plate fades into pale shades. Releasing the occlusion causes an increase and overshoot of the temperature by 9 °C within 100 s, coincident with an increase in blood flow above the initial value and a change in the color of the finger to red. Although the rapid, time dependent variations in temperature and blood flow frustrate precise analysis of the measurements, approximate values of the thermal conductivity of the nail bed tissue can be deduced with $k_1$ fixed to the average value of the measurement in Figure 5a. The thermal conductivity of the skin adjacent to the nail plate is measured with the sensor directly mounted on top of the skin, as indicated in the optical image in Figure 5c. Figure 5e shows that the conductivity decreases with occlusion, from $0.5 \pm 0.03$ to $0.44 \pm 0.02$ W m$^{-1}$ K$^{-1}$, corresponding to 14% change independent of the specific value of $k_1$ as in Figure 5f. Similar changes occur in the adjacent skin. Overall, changes in thermal conductivity track those in temperature, as expected in the case that the blood flow affects both temperature and thermal transport. The perfusion resulted

**ADVANCED
SCIENCE NEWS**
www.advancedsciencenews.com

**ADVANCED
FUNCTIONAL
MATERIALS**
www.afm-journal.de

**Figure 4.** Thermal characterization with a focus on the thermal conductivity of the bottom layer. a) Increases in temperature as a function of time for actuators with $R = 0.5$ mm and b) 1.5 mm on bilayer samples of Ecoflex (top layer, thickness = 0.3 mm) on bottom layers of different materials (Ecoflex, Sylgard567, Sylgard170, Sylgard164). c) FEA results for $T_{ss}$ as a function of $k_2$ for different values $k_1$. d) $\Delta T_{ss}/T_{ss}$ as a function of $\Delta k_2/k_2$ with different $k_1$. e) $\Delta T_{ss}/T_{ss}$ as a function of $\Delta k_2/k_2$ with different $k_2$. f) Comparison of $\Delta T_{ss}/T_{ss}$ as a function of $\Delta k_2/k_2$ from FEA and experimental results.

in changes in thermal conductivity, as further studied on two subjects (subject 1, previous female; subject 2, male at age 26, nail thickness $0.49 \pm 0.01$ mm, $k_1 = 0.26 \pm 0.01$ W m$^{-1}$ K$^{-1}$) before and after exercise. Thermal conductivity was measured for both subjects at rest before exercise (stationary bike for 15 min) and after, following a rest of 10 min. Figure 5f shows

that the thermal conductivity of the nailbed tissue increases after exercise for both subjects. The male subject shows an increase that is larger than that of the female subject, likely corresponding to elevated blood flow.[36]

A second demonstration of measurements on human subjects involves aspects related to thermoregulation.
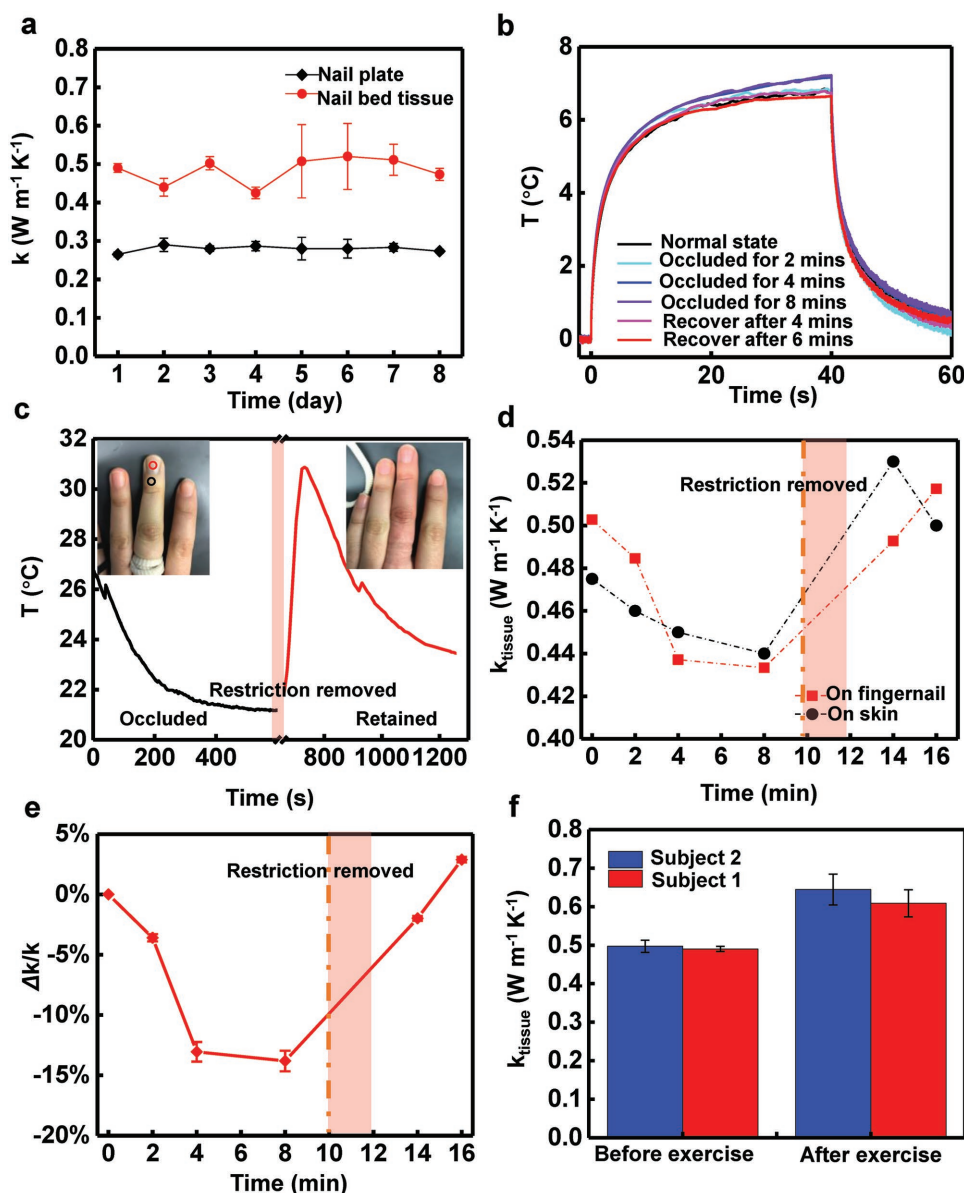
**Figure 5.** Results of thermal characterization studies on volunteer subjects. a) Thermal conductivity of the nail plate and nail bed tissue measured at room temperature each day for eight consecutive days. b) Time-dependent changes in temperature during before (<0 s), during (between 0 and 40 s), and after (>40 s) activation of a sensor with $R = 1.5$ mm on the left middle finger. c) Temperature of the fingernail of a subject determined using an infrared camera during and after occlusion of blood flow. d) Time-dependent changes in the thermal conductivity of the nail bed tissue and adjacent skin during and after occlusion. Measurement locations on the fingernail and adjacent skin are indicated by red and black circle in the inset in panel (c). e) Relative change in thermal conductivity $\Delta k_{nailbed}/k_{nailbed}$ of the nail bed tissue. f) Thermal conductivity changes of subject 1 and 2 before and after exercise.

Specifically, changes in the surrounding temperature can alter blood flow in deep tissues.[37] Here, studies involve two healthy subjects (previous female, and another male at age 30, with nail thickness of $0.51 \pm 0.01$ mm), each with their left middle finger placed on ice bag for 10 min. Procedures summarized in Figure 4a define the thermal conductivity of the nail plate ($k_{nail} = 0.28 \pm 0.03$ W m$^{-1}$ K$^{-1}$ for female and $k_{nail} = 0.26 \pm 0.02$ W m$^{-1}$ K$^{-1}$ for male); this value is assumed to remain constant. **Figure 6**a–e, presents measurement results and analysis of data from the female subject. During

the cooling period, the thermal conductivity of nail bed tissue decreases by ≈12%, likely a result of vasoconstriction induced by cooling. Removing the ice bag, and exercising the finger (rubbing and warm hand wash) for 6 min prepare the subject for a second set of measurements. During this process, the thermal conductivity of the nailbed recovers to a value ≈7% below the initial state after 6 min and only ≈2% below after 8 min. The results obtained from the male subject in Figure 6b,d,f show similar trends, but with a higher thermal conductivity and a larger change ≈30% compared to the female
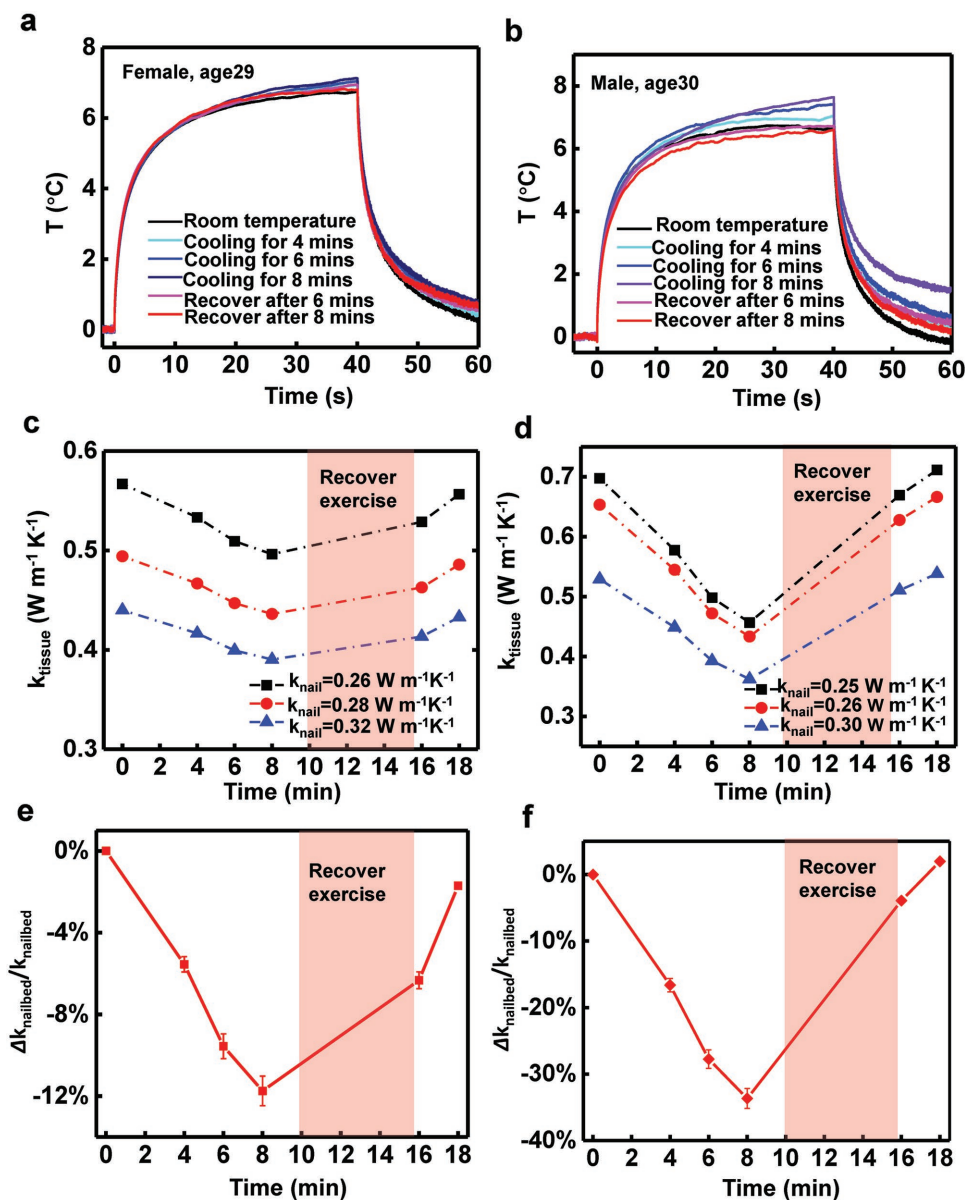
**Figure 6.** Studies of changes in thermal transport characteristics of the nailbed tissue associated with cooling the finger. a,b) Temperature responses associated with operation of a sensor with $R = 1.5$ mm measured on subject 1 (female, 29) and subject 2 (male, 30). c,d) Fitted thermal conductivity of the nailbed with $k_{nail}$ fixed to the minimum, mean, and maximum value of the thermal conductivity of the fingernail for each subject. e,f) Relative change in thermal conductivity, $\Delta k_{nailbed}/k_{nailbed}$, during and after cooling for each subject. The error bar corresponds to the deviation of the $\Delta k_{nailbed}/k_{nailbed}$ calculated using values of $k_{nail}$ in panels (c) and (d).

subject. After exercise, the male subject shows an increase of thermal conductivity of the nailbed tissue, the value reaches 5% below the one measured at the room temperature at 6 min and 2% above at 8 min.

## 3. Conclusion

The results presented here establish a general set of materials, device structures, measurement approaches, and analysis techniques for noninvasive characterization of the thermal properties of systems consisting of a thin layer of material on top of a semi-infinite substrate, specifically modeled after the nail/nailbed structures of the human body. Measurements on a range of synthetic analogs to fingernails highlight the key considerations and define the optimized modes of analysis. Evaluations on human subjects illustrate possibilities for tracking changes in perfusion in the nailbed tissue via measurements from the surface of the nail plate. Future work will explore advanced sensor layouts to enhance the measurement precision and capabilities in depth profiling of the transport characteristics. Addition of other types of sensors, such as

optical devices for determining blood oxygenation and capturing photoplethysograms, will yield multimodal platforms for tracking physiological health status. These and other opportunities, taken in the context of the advantages of the nail plate as a point of device integration with the body, suggest many fruitful directions for further research and engineering development.

## 4. Experimental Section

*Device Fabrication*: Fabrication and design details are in the Supporting Information. Briefly, the process starts with spin casting a thin sacrificial layer of (poly)methyl-methacrylate (PMMA Microchem, Westborough, MA) on a clean silicon wafer. A film of polyimide (PI 2545, Parlin, NJ, 3 µm thick) spin-cast and cured on the top of this layer forms the bottom side of the encapsulation. A bilayer of Cr (10 nm)/Au (100 nm) deposited on top of the polyimide by electron beam evaporation and then patterned by photolithography and wet etching forms the conducting traces for the devices. The use of wide interconnect lines minimizes their resistances. A second layer of PI layer formed by spin casting and curing yields the top encapsulation. Photolithography and etching the PI defines the outline of the sensor. Immersing the wafer in acetone removes the underlying PMMA, thereby releasing the sensors from the wafer. Retrieval using a polyvinyl alcohol (PVA)-based water soluble tape (3M, Minneapolis, MN) followed by deposition of a thin layer of $SiO_2$ facilitates adhesive bonding to a thin (50 µm) silicone-based substrate (Ecoflex, Smooth-On Inc., Macungie, PA). Removing the PVA by immersion in warm water completes the fabrication.

*Measurement Scheme*: The sensors connect with a flexible cable to a custom printed circuit board as an interface to the measurement hardware. A precision DC current source (Keithley 6220, USA) supplies a constant current to the sensors and a DMM (National Instrument, USA) records the voltages. Instrument control and Data acquisition are performed using a custom computer program (LabVIEW, National Instruments, USA) via a GPIB-USB interface. Consent was obtained from the human subjects participating in the experiments.

## Supporting Information

Supporting Information is available from the Wiley Online Library or from the author.

## Conflict of Interest

The authors declare no conflict of interest.

[1] M. N. Zaiac, A. Walker, *Clin. Dermatol.* **2013**, *31*, 627.
[2] K. N. Shah, A. I. Rubin, *Curr. Probl. Pediatr. Adolesc. Health Care* **2012**, *42*, 204.
[3] R. S. Fawcett, S. Linford, D. L. Stulberg, *Am. Fam. Physician* **2004**, *69*, 1417.
[4] M. Cutolo, C. Pizzorni, M. E. Secchi, A. Sulli, *Best Pract. Res. Clin. Rheumatol.* **2008**, *22*, 1093.
[5] L. Thomas, E. G. Zook, E. Haneke, J.-L. Drapé, R. Baran, J. F. Kreusch, in *Baran & Dawber's Diseases of the Nails and their Management* (Eds: R. Baran, D. A. R. de Berker, M. Holzberg, L. Thomas), Wiley-Blackwell, Hoboken, NJ, USA **2012**, pp. 637–743.
[6] C. Grover, S. Bansal, *Indian Dermatol. Online J.* **2018**, *9*, 3.
[7] T. E. Rohrer, B. Leslie, D. J. Grande, *J. Dermatol. Surg. Oncol.* **1994**, *20*, 19.
[8] R. H. Rice, Y. Xia, R. J. Alvarado, B. S. Phinney, *J. Proteome Res.* **2010**, *9*, 6752.
[9] S. Yaemsiri, N. Hou, M. M. Slining, K. He, *J. Eur. Acad. Dermatol. Venereol.* **2010**, *24*, 420.
[10] R. C. Webb, Y. Ma, S. Krishnan, Y. Li, S. Yoon, X. Guo, X. Feng, Y. Shi, M. Seidel, N. H. Cho, J. Kurniawan, J. Ahad, N. Sheth, J. Kim, J. G. T. Vi, T. Darlington, K. Chang, W. Huang, J. Ayers, A. Gruebele, R. M. Pielak, M. J. Slepian, Y. Huang, A. M. Gorbach, J. A. Rogers, *Sci. Adv.* **2015**, *1*, e1500701.
[11] R. C. Webb, R. M. Pielak, P. Bastien, J. Ayers, J. Niittynen, J. Kurniawan, M. Manco, A. Lin, N. H. Cho, V. Malyrchuk, G. Balooch, J. A. Rogers, *PloS One* **2015**, *10*, e0118131.
[12] R. C. Webb, A. P. Bonifas, A. Behnaz, Y. Zhang, K. J. Yu, H. Cheng, M. Shi, Z. Bian, Z. Liu, Y.-S. Kim, W.-H. Yeo, J. S. Park, J. Song, Y. Li, Y. Huang, A. M. Gorbach, J. A. Rogers, *Nat. Mater.* **2013**, *12*, 938.
[13] S. Amendola, G. Bovesecchi, P. Coppa, G. Marrocco, in *2016 IEEE International Symposium on Antennas and Propagation (APSURSI)*, Fajardo, Puerto Rico, USA **2016**, pp. 461–462.
[14] S. E. Gustafsson, *Rev. Sci. Instrum.* **1991**, *62*, 797.
[15] M. Johnson, S. Shuster, *Br. J. Dermatol.* **1994**, *130*, 195.
[16] J. B. Hamilton, H. Terada, G. E. Mestler, *J. Gerontol.* **1955**, *10*, 401.
[17] U. Wollina, M. Berger, K. Karte, *Skin Res. Technol.* **2001**, *7*, 60.
[18] D. T. Dias, A. Steimacher, A. C. Bento, A. M. Neto, M. L. Baesso, *Photochem. Photobiol.* **2007**, *83*, 1144.
[19] T. E. Cooper, G. J. Trezek, *Aerosp. Med.* **1971**, *42*, 24.
[20] T. A. Balasubramaniam, H. F. Bowman, *J. Biomech. Eng.* **1977**, *99*, 148.
[21] W. J. B. M. van de Staak, A. J. M. Brakkee, H. E. de Rijke-Herweijer, *J. Invest. Dermatol.* **1968**, *51*, 149.
[22] A. Chanmugam, A. Bhargava, C. Herman, *Int. Mech. Eng. Congr. Expo.* **2012**, *2*, 717.
[23] A. M. Stoll, *J. Invest. Dermatol.* **1977**, *69*, 328.
[24] A. Sizov, D. Cederkrantz, L. Salmi, A. Rosén, L. Jacobson, S. E. Gustafsson, M. Gustavsson, *Rev. Sci. Instrum.* **2016**, *87*, 74901.
[25] *Thermal Conductivity: Theory, Properties, and Applications* (Ed: T. M. Tritt), Physics of Solids and Liquids, Springer, New York, NY, US **2004**.
[26] A. R. Moritz, F. C. Henriques, *Am. J. Pathol.* **1947**, *23*, 695.
[27] J. P. Bull, J. C. Lawrence, *Fire Mater.* **1979**, *3*, 100.

[28] *Dow Corning Sylgard170 Silicone Elastomer Product Information*, Dow Corning, **2017**, https://consumer.dow.com/documents/en-us/productdatasheet/11/11-31/11-3181-sylgard-170-silicone-elastomer.pdf?iframe=true.

[29] L. Tian, Y. Li, R. C. Webb, S. Krishnan, Z. Bian, J. Song, X. Ning, K. Crawford, J. Kurniawan, A. Bonifas, J. Ma, Y. Liu, X. Xie, J. Chen, Y. Liu, Z. Shi, T. Wu, R. Ning, D. Li, S. Sinha, D. G. Cahill, Y. Huang, J. A. Rogers, *Adv. Funct. Mater.* **2017**, *27*, 1701282.

[30] T. H. Benzinger, A. W. Pratt, C. Kitzinger, *Proc. Natl. Acad. Sci. USA* **1961**, *47*, 730.

[31] R. Refinetti, *Exp. Physiol.* **2003**, *88*, 423.

[32] A. Dittmar, T. Pauchard, G. Delhomme, E. Vernet-Maury, *Sens. Actuators, B* **1992**, *7*, 327.

[33] M. Salcman, E. Moriyama, H. J. Elsner, H. Rossman, R. A. Gettleman, G. Neuberth, G. Corradino, *J. Neurosurg.* **1989**, *70*, 592.

[34] J. Grayson, *J. Physiol.* **1952**, *118*, 54.

[35] R. K. Jain, F. H. Grantham, P. M. Gullino, *J. Natl. Cancer Inst.* **1979**, *62*, 927.

[36] J. Bangsbo, Y. Hellsten, *Acta Physiol. Scand.* **1998**, *162*, 305.

[37] H. Barcroft, O. G. Edholm, *J. Physiol.* **1943**, *102*, 5.